A Novel Modular Positive-Sequence Synchrophasor Estimation Algorithm for PMUs

Francisco Messina, *Student Member, IEEE*, Pablo Marchi, *Student Member, IEEE*, Leonardo Rey Vega, *Member, IEEE*, Cecilia G. Galarza, and Héctor Laiz

***Abstract*— A novel modular positive-sequence estimation algorithm for phasor measurement units (PMUs) is described in this paper with a focus on the restrictions imposed by the IEEE C37.118.1-2011 standard. The first stage consists in a three-phase demodulator which allows us to separate the positive-sequence from the negative-sequence signal in the frequency domain and to eliminate the zero-sequence signal. The second stage is a prefilter that mitigates noise and interference, thus relaxing the filtering requirements of the following stage. The suitability of a linear-phase FIR filter is shown and a comparison of single and multistage designs is presented. On the third stage, a digital state-space-based extension of a synchronous reference frame-phase-locked loop is used for tracking of amplitude, phase, frequency, and rate of change of frequency. It is shown that a phase predictor inside the loop is required. The fourth stage is a compensation algorithm which takes into account the narrowband nature of the input signal to perform an accurate compensation of the filter effects on the signal of interest. Analytical properties of the system are then presented, providing insight into the main factors that affect global performance. Finally, a strict evaluation of the system is presented for both M and P class PMU.**

***Index Terms*— IEEE standards, linear-phase filters, phase-locked loops (PLLs), phasor measurement units (PMUs), system analysis and design.**

I. Introduction

PHASOR measurement units (PMUs) are considered a fundamental component of the Smart Grid, a contemporary perspective which promises to give power systems a new level in terms of reliability and efficiency [1]. The main advantage of this technology with respect to traditional SCADA systems is that their measurements are time-stamped using a reference synchronization signal, generally provided by a Global Positioning System receiver, and are taken much faster. In this way, PMUs can yield phase information with much greater accuracy. This feature also allows to integrate many PMU measurements for new applications, such as real-time state estimation, fault detection, and robust control of wide area systems. The IEEE Standard C37.118.1-2011 [2] on synchrophasors and its recent amendment C37.118.1a-2014 [3] establish requirements on PMUs to ensure a minimal performance and interoperability between different devices. From now on, these will simply be referred to as the IEEE Standard for brevity.

Phasor estimation was traditionally performed with a DFT recursive algorithm for its efficiency and great harmonic rejection capability [4]. However, this method does not perform well for off-nominal frequencies because of the well-known leakage effects: scalloping loss and spectral interference. A suitable window selection can greatly reduce spectral interference [5], while interpolation algorithms have been proposed to cope with the scalloping loss problem [6]. However, these approaches still have several limitations. First, they provide poor filtering of interharmonic signals. Second, they do not provide direct estimations of frequency and rate of change of frequency (ROCOF), which means that numerical differentiation must be performed on the phase estimated sequence. Since the simple finite differences method is not accurate enough, a careful *ad hoc* design of differentiator filters is required. Third, they are generally not well-suited for dynamic signals since they are based on a stationary model.

A dynamic phasor model based on the Taylor's series expansion led to several extensions of the DFT algorithm [7]. In [8], the first and second-order models are introduced, yielding, respectively, the 4PM and 6PM algorithms. Alternatively, the estimation can be performed through least squares (LSs) [9] or weighted LSs procedures [10] based on the dynamic model. A detailed comparison of these algorithms can be found in [11]–[13]. Although these approaches provide generally better performance than stationary algorithms, interference rejection remains to be a problem as can be seen in the reported numerical results [12]. More importantly, they lack a simple way to control different aspects of estimation performance.

A different approach to this problem is the use of a phase-locked loop (PLL), which is a well-suited system for dynamic tracking that is controlled by a simple parameterization [14]. Much research has been done in this area for adapting PLLs for power system applications, both for single- and three-phase systems. The basic three-phase PLL is known as the synchronous reference frame PLL (SRF-PLL) and allows to obtain a ripple free phase detector (PD) when the input signal is balanced [15]. More complex PD schemes which attempt to achieve this for unbalanced signals gave rise to different PLLs such as the enhanced PLL (EPLL) [15] and the

Manuscript received July 11, 2016; revised September 6, 2016; accepted October 10, 2016. Date of publication December 30, 2016; date of current version May 10, 2017. This work was supported in part by the UREE 4 FONARSEC Project: "Development of Synchrophasor Measurements for Smart Electrical Grids" from the Ministry of Science, Technology and Innovation of Argentina. The work of F. Messina was supported by a Peruilh Ph.D. grant from the Universidad de Buenos Aires. The Associate Editor coordinating the review process was Dr. Carlo Muscas.

F. Messina, P. Marchi, L. Rey Vega, and C. G. Galarza are with the Centro de Simulación Computacional, Consejo Nacional de Investigaciones Científicas y Técnicas, and Universidad de Buenos Aires (e-mail: fmessina@fi.uba.ar).

H. Laiz is with the Instituto Nacional de Tecnología Industrial (INTI), Buenos Aires, Argentina, and also with the Instituto de la Calidad Industrial (INCALIN), Universidad Nacional de San Martín, Buenos Aires 1650, Argentina.

Digital Object Identifier 10.1109/TIM.2016.2637578

decoupled double SRF PLL (DDSRF-PLL) [16]. Typically, the design difficulty of these systems lies on the tradeoff between a fast dynamic response and filtering performance. On the one hand, to obtain a fast dynamical response, a large enough bandwidth is required. On the other hand, to filter unwanted signals, bandwidth should be reduced as much as possible. This yields a tight constraint, which cannot be fulfilled with standard configurations [14], [15], but can be alleviated by a properly designed prefiltering stage.

The purpose of this paper is to present a novel integration of different techniques to obtain a coherent, complete, and robust positive-sequence synchrophasor estimation algorithm for PMUs based on a PLL and a prefiltering stage. Although similar structures have been considered before in power system applications [15], they are generally not suitable for PMUs for several reasons. First, use of simple IIR prefilters (PFs) is proposed, but this causes phase distortion which leads to significant total vector error (TVE) values. We precisely characterize the group delay requirements of this stage to show how critical is this issue, which almost dictates that an FIR PF should be used. Second, PLLs are typically introduced in the continuous-time domain and their discretization analysis neglected. However, finite delays inside the loop can be harmful. In fact, we show that a linear predictor scheme is required. In addition, we apply the recently introduced narrowband compensation algorithm (NCA) algorithm [17], which takes into account the finite bandwidth of the information signal to more accurately compensate the filtering effects. Furthermore, we present several analytical properties which prove to be useful for the design validation of the complete system and provide insight into the main factors that affect its performance. This also reduces the tedious and time consuming trial-and-error procedure required for parameter selection.

The rest of this paper is organized as follows. In Section II, the signal model and the proposed system are presented. The three-phase demodulation scheme is briefly discussed in Section III. Then, in Section IV, the PF stage design considerations are presented and both single and multistage designs are investigated. A state-space based estimator-predictor extension to the classical SRF-PLL is presented in Section V. The compensation algorithm is reviewed in Section VI. System properties are given in Section VII. Extensive simulation results are presented in Section VIII for two cases: an M class PMU with reporting rate $F_s = 10$ fps and a P class PMU with reporting rate $F_s = 50$ fps. Finally, the conclusions are drawn in Section IX.

II. Signal Model and System Architecture

Since the focus of this paper is on the digital stage design, we will work in the discrete-time domain. That is, we will assume that current and voltage signals are digitally sampled by an analog-to-digital-converter (with a properly designed antialiasing filter) with a sampling time T. A sampled version of a continuous-time signal $x(t)$ will be represented as $x[n] \equiv x(nT)$ with $n \in \mathbb{Z}$. The effects of the analog stage are only considered briefly in Section VI for compensation purposes. However, the system analysis could be simply extended to account for these effects in a practical case.

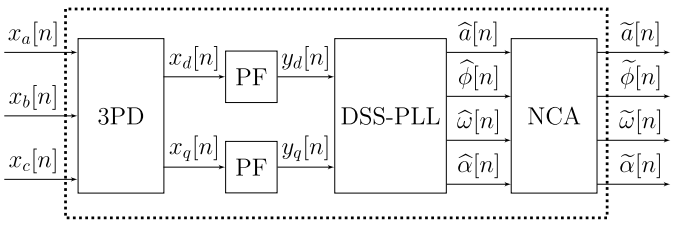

Fig. 1. PMU digital stage block diagram.

In general, the fundamental component of the three-phase input signal may be written as the sum of the instantaneous symmetrical components [18] as in (1), shown at the bottom of this page, where $a_i[n] \equiv a_i(nT)$ and $\phi_i[n] \equiv \phi_i(nT)$, $i = a, b, c, 0, 1, 2$, are the instantaneous amplitude and phase of the corresponding phase or sequence component, ω_0 is the nominal angular frequency of the power system, and $T = 2\pi/(K\omega_0)$ is the sampling period, with K an arbitrary integer greater than 2. In this paper, we will assume that signals in (1) may be represented as narrowband passband signals within the delay of the system at nominal frequency of operation. A similar assumption is made in [7]. Also, the central frequency ω is assumed to lie in the interval $[\omega_0 - B/2, \omega_0 + B/2]$, where B is the range of frequencies of interest, which is generally small relative to ω_0. Note that the input signal to the system will be actually composed of other narrowband components (harmonics and interharmonics) and wideband noise which are omitted just for notational brevity.

As stated, we focus on the positive-sequence signal estimation problem, that is, the objective is to track the positive-sequence phasor, frequency, and ROCOF. If desired, the estimation of the negative-sequence quantities can be obtained by a trivial extension of the proposed system. Instead, for the zero-sequence component tracking, a single-phase system based on an EPLL could be used. Nevertheless, requirements for these other systems are not as well established.

The complete block diagram of the proposed system is shown in Fig. 1. It includes a three-phase demodulator (3PD), one digital PF for each signal branch (d and q), a digital state-space PLL (DSS-PLL), and a NCA block. The three-phase demodulation transforms the positive-sequence signal into a lowpass signal (i.e., centered around 0 Hz) and separates it from the negative-sequence signal in the frequency domain. The PF is used to relax the specifications of the PLL's loop filter design, since it is not possible to obtain both a fast dynamic response and interference rejection with the standard configurations [15]. Of course, more complex in-loop filters

$$\mathbf{x}_{abc}[n] = \begin{bmatrix} x_a[n] \\ x_b[n] \\ x_c[n] \end{bmatrix} = a_0[n] \begin{bmatrix} \cos(\omega_0 nT + \phi_0[n]) \\ \cos(\omega_0 nT + \phi_0[n]) \\ \cos(\omega_0 nT + \phi_0[n]) \end{bmatrix} + a_1[n] \begin{bmatrix} \cos(\omega_0 nT + \phi_1[n]) \\ \cos\left(\omega_0 nT + \phi_1[n] - \frac{2\pi}{3}\right) \\ \cos\left(\omega_0 nT + \phi_1[n] + \frac{2\pi}{3}\right) \end{bmatrix} + a_2[n] \begin{bmatrix} \cos(\omega_0 nT + \phi_2[n]) \\ \cos\left(\omega_0 nT + \phi_2[n] + \frac{2\pi}{3}\right) \\ \cos\left(\omega_0 nT + \phi_2[n] - \frac{2\pi}{3}\right) \end{bmatrix} \quad (1)$$

could be used to try to solve the joint filtering and tracking problem [19]. However, it is noted that its design and global stability considerations are not simple to pose. Instead, in this paper, we propose to solve the filtering problem in the signal domain and the tracking problem in the phase domain. This is much simpler, as it allows us to decouple these problems and to perform a detailed analysis in each domain. In turn, this provides valuable insights into the interrelationship of these two tasks. The tracking task is covered by the DSS-PLL, which is an estimator-predictor PLL [20], that arises from a natural state-space extension of the SRF-PLL. A similar state-space approach to the problem was considered in [21]. The proposed PLL tracks effectively amplitude, phase, frequency, and ROCOF. Finally, we present the NCA, which accurately corrects for the gain, phase, and delay introduced in the filtering stages (both analog and digital) of the system [17]. It is worth emphasizing that each of these blocks is critical to ensure correct PMU operation.

III. Three-Phase Demodulation

The three-phase demodulation can be performed with a standard abc-dq or Park transform [22] (the zero component is not computed since it does not provide positive-sequence information)

$$\boldsymbol{P}[n] = \frac{2}{3}\begin{bmatrix} \cos\left(\phi_a^0[n]\right) & \cos(\phi_b^0[n]) & \cos(\phi_c^0[n]) \\ -\sin\left(\phi_a^0[n]\right) & -\sin(\phi_b^0[n]) & -\sin(\phi_c^0[n]) \end{bmatrix}$$

where $\phi_a^0[n] = \omega_0 nT$, $\phi_b^0[n] = \omega_0 nT - 2\pi/3$, and $\phi_c^0[n] = \omega_0 nT + 2\pi/3$. Then, $\mathbf{x}_{dq}[n] = \boldsymbol{P}[n]\,\mathbf{x}_{abc}[n]$ gives

$$\mathbf{x}_{dq}[n] = a_1[n]\begin{bmatrix}\cos(\phi_1[n])\\ \sin(\phi_1[n])\end{bmatrix} + a_2[n]\begin{bmatrix}\cos(2\omega_0 nT+\phi_2[n])\\ -\sin(2\omega_0 nT+\phi_2[n])\end{bmatrix}.$$

This transformation offers many advantages.

1) Unlike a single-phase demodulation, it avoids the creation of double-frequency terms for balanced input signals.
2) It completely filters out the zero-sequence component.
3) While the positive-sequence frequency is shifted to dc, the negative-sequence component frequency is shifted to $2\omega_0$. This double-frequency term will be filtered by the PF, so that proper ripple free operation of the PLL is guaranteed even in unbalanced scenarios. For severely distorted signals, a carefully designed notch filter could be added to relax the PF requirements.

Note that harmonics and interharmonics components can be analyzed similarly. Therefore, positive-sequence interference signals are shifted in frequency by $-\omega_0$, negative-sequence interference signals are shifted by $+2\omega_0$, and zero-sequence interference signals are eliminated. This will simply change the interference power frequency distribution.

IV. Prefilter Design Considerations

We start by studying the PMU tolerance to PF phase distortion. Concretely, we will analyze the TVE generated by the variation of the PF group delay with frequency. Let $H_{\mathrm{PF}}(z)$ be the PF transfer function, $G_{\mathrm{PF}}(\nu)$ be the magnitude response, $\phi_{\mathrm{PF}}(\nu)$ be the phase response, and $\tau_{\mathrm{PF}}(\nu)$ be the group delay in time units, where ν is the discrete-time frequency variable.[1] In general, the PF outputs are

$$\mathbf{y}_{dq}[n] = \begin{bmatrix} y_d[n] \\ y_q[n] \end{bmatrix} = \begin{bmatrix} (h_{\mathrm{PF}} * x_d)[n] \\ (h_{\mathrm{PF}} * x_q)[n] \end{bmatrix} = a[n]\begin{bmatrix}\cos(\phi[n])\\ \sin(\phi[n])\end{bmatrix}$$

where $a[n] = (y_d^2[n] + y_d^2[n])^{1/2}$ and $\phi[n] = \mathrm{atan2}(y_q[n], y_d[n])$, being atan2 the four-quadrant inverse tangent function. Using the narrowband assumption, we readily obtain the following approximations:

$$a[n] \approx G_{\mathrm{PF}}(\eta)a_1(nT - \tau_{\mathrm{PF}}(\eta)),$$
$$\phi[n] \approx \phi_1(nT - \tau_{\mathrm{PF}}(\eta)) + \phi_{\mathrm{PF}}(\eta) + \frac{\eta}{T}\tau_{\mathrm{PF}}(\eta)$$

where $\eta = \Delta\omega\, T$ and $\Delta\omega = \omega - \omega_0$. Now, we investigate the error produced by considering $\tau_{\mathrm{PF}}(\eta) \approx \tau_{\mathrm{PF}}^0$ for all $\eta \in \Omega_p = [-BT/2, BT/2]$, where τ_{PF}^0 is the nominal group delay (constant approximation). This approximation is extremely important in order to allow for a simple compensation procedure of the system delay, which proves to be critical (see Section VI). It can be simply shown that phase error (PE) and amplitude error (AE) may be bounded as

$$\mathrm{PE}(\eta) \le \mu_\phi\, \Delta\tau_{\mathrm{PF}}(\eta), \qquad \mathrm{AE}(\eta) \le \mu_a G_{\mathrm{PF}}(\eta)\Delta\tau_{\mathrm{PF}}(\eta)$$

where $\Delta\tau_{\mathrm{PF}}(\eta) = \tau_{\mathrm{PF}}(\eta) - \tau_{\mathrm{PF}}^0$, μ_ϕ is an upper bound for $[\Delta\omega - \phi_1'(nT - \tau_{\mathrm{PF}}^0)]$, and where μ_a is an upper bound for $a_1'(nT - \tau_{\mathrm{PF}}^0)$. Generally, AE is negligible and $\mathrm{PE}(\eta) \ll 1$ rad. for all $\eta \in \Omega_p$, so that

$$\mathrm{TVE} = \sup_{\eta\in\Omega_p} |[1 + \mathrm{AE}(\eta)]\, e^{j\,\mathrm{PE}(\eta)} - 1| \approx \sup_{\eta\in\Omega_p} |\mathrm{PE}(\eta)| \le \mu_\phi \sup_{\eta\in\Omega_p} |\Delta\tau_{\mathrm{PF}}(\eta)|. \quad (2)$$

It is important to observe that the above upper bound includes two effects. The term μ_ϕ is related to the variability of the phase of the input signal while $\sup_{\eta\in\Omega_p}|\Delta\tau_{\mathrm{PF}}(\eta)|$ is the PF group delay dispersion, which can be controlled by the system designer. Since TVE should be much less than 1%, we can use (2) to obtain an upper bound for the group delay dispersion. For example, by using the passband definition for the M class PMU, $\mu_\phi = 2\pi \times 5$ rad/s, we obtain the condition $|\Delta\tau_{\mathrm{PF}}(\nu)| \ll 0.01/(10\pi) = 318\ \mu$s for all $\nu \in \Omega_p$. For typical values of T, this result shows that group delay dispersion must be only a small fraction of a sample,[2] so that the PF phase characteristic is a critical design issue. This requirement is easily achieved with FIR linear-phase filters which have a constant group delay. There are also interesting quasi-linear-phase IIR design algorithms that could be used such as those in [23], based on convex optimization, but this will not be pursued further here. Note that a similar analysis should be performed for the analog stage of an actual PMU.

The lowpass PF magnitude specifications are given by the usual four parameters: the passband edge frequency f_p, the stopband edge frequency f_s, the passband ripple δ_p, and the stopband attenuation δ_s. Guidelines for the selection of

[1] This notation is used throughout this paper: for any transfer function $H(z)$, its magnitude response is denoted by $G(\nu)$ and its phase response as $\phi(\nu)$.

[2] For example, sampling a 50-Hz signal with 28 samples per cycle will require $T \approx 714\ \mu$s.

TABLE I
MULTISTAGE PF CHARACTERISTICS

	M class		P class	
# Stages	C	τ_{PF} [ms]	C	τ_{PF} [ms]
1	1183	422	59	21
2	125	472	25	26
3	87	500	28	32
4	88	513	38	42
5	96	534	43	47

these parameters are readily obtained from the IEEE Standard specifications. The single-stage optimal filter (in terms of computational cost and delay), the equiripple filter, can be designed with the Parks–McClellan algorithm and it has a cost which can be obtained approximately with the empirical Kaiser's formula [24]

$$C \approx \frac{-10\log_{10}(\delta_p\delta_s) - 13}{14.6\,\Delta f\,T} \tag{3}$$

where $\Delta f = f_s - f_p$. The cost (or order N) of the single-stage FIR PFs given by (3) is relatively large, particularly for M class specifications which have a very narrow transition band. An efficient method to design a multistage filter is the IFIR approach [25], which consists in designing the filter in two stages: an upsampled filter with a factor M and an image suppresor filter. The total filter cost C can be found as the sum of the costs of each filter

$$C \approx \frac{-10\log_{10}(\delta_p\delta_s/2) - 13}{14.6\,M\Delta f T} + M\frac{-10\log_{10}(\delta_p\delta_s/2) - 13}{14.6\,(1 - M(f_s + f_p)T)}.$$

By minimizing this expression with respect to $M \in \mathcal{M} = \{2, \ldots, \lfloor (2f_sT)^{-1} \rfloor\}$, one finds the most efficient two-stage filter. The method is easily extended to the design of filters with more than two stages by "splitting" the last filter successively. We summarize the results[3] for both M and P class PF designs from one up to five stages in Table I. Note the great reduction in computational cost that can be achieved by a multistage design, especially for the M class PF, at the expense of minor increases in delay and associated memory requirements. The frequency responses of a four-stage M class PF and a two-stage P class PFs[4] are shown in Fig. 2.

V. TRACKING SYSTEM: DSS-PLL

The DSS-PLL extends the standard SRF-PLL by introducing a state-space model for amplitude, phase, frequency, and ROCOF. In this way, it provides naturally the loop filter structure, discretization process, and predictor scheme. Moreover, it can be simply generalized if desired. For a similar approach to the problem, see [21]. A complete block diagram of the DSS-PLL is shown in Fig. 3. In the following, a detailed description of each block is given.

[3]Note that the cost of the filter C and the filter order N is equal for single-stage filters but in general differ for multistage filters. The delay is always related to the latter quantity by the relation $\tau_{\text{PF}} = NT/2$.

[4]Filter specifications are as follows. For the M class PF, we have used $f_p = 2$ Hz, $f_s = 5$ Hz, $\delta_p = 10^{-3}$, and $\delta_s = 10^{-2}$. Instead, for the P class PF, we have used $f_p = 2$ Hz, $f_s = (48\times 2 - 50) = 46$ Hz, $\delta_p = 10^{-3}$, and $\delta_s = 10^{-2}$. This relatively small value for δ_s for the P class filter is used because of the harmonic distortion RFE stringent requirement.

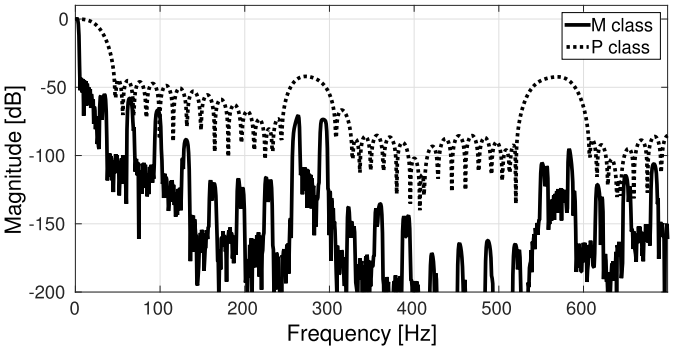

Fig. 2. Magnitude response of multistage PFs.

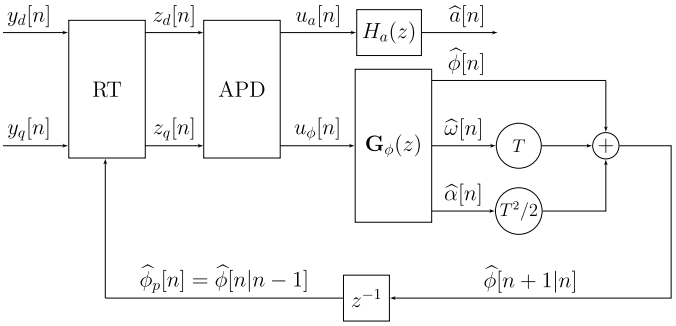

Fig. 3. DSS-PLL block diagram.

A. Rotation Transformation

As it has been already mentioned, the SRF-PLL gives a ripple free PD for balanced signals. This is achieved by exploiting its symmetry with the well-known Park's transformation. In the case where signals are unbalanced, its performance is seriously deteriorated [15], [16]. However, as discussed earlier, the proposed system can completely eliminate the zero-sequence component and sufficiently mitigate the negative-sequence double-frequency component. Thus, even when the input signal is distorted, the input to the DSS-PLL will contain only a small amount of interference, so that this approach remains useful. Since the input signal is already in the dq reference frame, we simply need a rotation transformation (RT). Let $\widehat{\phi}_p[n] = \widehat{\phi}[n|n-1]$ be the one-step current predicted phase by the DSS-PLL. Then, the RT $\boldsymbol{R}[n]$ yields

$$\mathbf{z}_{dq}[n] = a[n]\begin{bmatrix}\cos(\phi[n] - \widehat{\phi}_p[n])\\ \sin(\phi[n] - \widehat{\phi}_p[n])\end{bmatrix} + \mathbf{n}_{dq}[n]$$

where $\boldsymbol{R}[n]$ is a clockwise rotation matrix by the angle $\widehat{\phi}_p[n]$, and $\mathbf{n}_{dq}[n] = \boldsymbol{R}[n]\,\mathbf{v}_{dq}[n]$, being $\mathbf{v}_{dq}[n]$ remnant interference and noise after the PF stage. Since the difference between $\widehat{\phi}_p[n]$ and $\widehat{\phi}[n]$ is negligible (see Section V-D), the DSS-PLL effectively tracks $\phi[n]$ as desired.

B. Amplitude and Phase Detection

Unlike most works, both $z_d[n]$ and $z_q[n]$ signals are used to perform a joint amplitude and phase detection (APD) as

$$u_a[n] = \sqrt{z_d^2[n] + z_q^2[n]}, \quad u_\phi[n] = \text{atan2}(z_q[n], z_d[n]).$$

This makes the system much more robust against large phase jumps and amplitude sags/swells, since it provides a better decoupling than the one obtained when $z_d[n]$ and $z_q[n]$ are used separately. Moreover, it provides a linear phase characteristic between $-\pi$ and π, which yields better tracking performance than the sinusoidal PD [26]. For high signal-to-interference-plus-noise ratio values, which are guaranteed by the PF stage, it can be shown that this detection scheme does not amplify the power of $\mathbf{n}_{dq}[n]$. In fact, a first-order approximation gives

$$u_a[n] \approx a[n] + n_a[n], \quad u_\phi[n] \approx \phi[n] - \widehat{\phi}_p[n] + n_\phi[n]$$

where the total power of $n_a[n]$ and $n_\phi[n]$ is the same as that of $n_d[n]$ and $n_q[n]$.

C. Loop Filter Structure

The discussion in this section starts in the continuous-time domain for the clarity of presentation. As previously mentioned, instead of using a standard PI filter, the loop filter of the DSS-PLL is obtained from a state observer of the following state-space model:

$$\begin{cases} \mathbf{x}'_\phi(t) = \boldsymbol{A}_\phi\, \mathbf{x}_\phi(t) \\ y_\phi(t) = \mathbf{c}_\phi^T \mathbf{x}_\phi(t), \end{cases} \qquad \boldsymbol{A}_\phi = \begin{bmatrix} 0 & 1 & 0 \\ 0 & 0 & 1 \\ 0 & 0 & 0 \end{bmatrix}, \ \mathbf{c}_\phi = \begin{bmatrix} 1 \\ 0 \\ 0 \end{bmatrix} \tag{4}$$

where the state vector is $\mathbf{x}_\phi(t) = [\phi(t), \omega(t), \alpha(t)]^T$, being $\phi(t)$ the phase of the input signal, $\omega(t) = \phi'(t)$, $\alpha(t) = \phi''(t)$, and the output $y_\phi(t) = \phi(t)$. The assumed state matrix $\boldsymbol{A}_\phi$ implies that $\phi'''(t) = 0$, i.e., ROCOF is constant. The state observer of this model yields a standard type 3 PLL. As is well-known in the PLL literature, this is the minimum type required to track frequency ramps without steady-state error [27], [28]. One disadvantage of the previous model is that it is not exact for modulated signals. For example, for sinusoidal phase modulation $\phi'''(t) = a\,\phi'(t)$ for some $a \neq 0$. A more general model that accounts for these signals would imply that the third row of the state matrix in (4) is replaced by $[a, b, c]$ where $a, b, c \in \mathbb{R}$ are not necessarily zero. However, this model requires an accurate online model identification, which introduces additional stability and performance issues. Moreover, as it will be shown through numerical simulations in Section VIII, the errors of the simpler model for phase modulation signals can be made small enough. Thus, model (4) will be used in this paper.

The corresponding discrete-time state-space model is

$$\begin{cases} \mathbf{x}_\phi[n+1] = e^{\boldsymbol{A}_\phi T}\, \mathbf{x}_\phi[n] \\ y_\phi[n] = \mathbf{c}_\phi^T \mathbf{x}_\phi[n], \end{cases} \qquad e^{\boldsymbol{A}_\phi T} = \begin{bmatrix} 1 & T & T^2/2 \\ 0 & 1 & T \\ 0 & 0 & 1 \end{bmatrix}.$$

Let $\widehat{\mathbf{x}}_\phi[l|m]$ represent the estimate of $\mathbf{x}_\phi[l]$ at time m. For the sake of notational simplicity, $\widehat{\mathbf{x}}_\phi[m|m]$ is simply denoted by $\widehat{\mathbf{x}}_\phi[m]$. The current observer equation can then be written as

$$\widehat{\mathbf{x}}_\phi[n] = e^{\boldsymbol{A}_\phi T} \widehat{\mathbf{x}}_\phi[n-1] + \mathbf{k}(y_\phi[n] - \mathbf{c}^T e^{\boldsymbol{A}_\phi T} \widehat{\mathbf{x}}_\phi[n-1])$$

where $\mathbf{k} = [k_1, k_2, k_3]^T$ is the vector gain. The open-loop phase transfer function which produces the state estimation in response to $u_\phi[n]$ is given by (5) at the bottom of this page. The corresponding closed-loop transfer functions between $\phi[n]$ and $\widehat{\phi}[n]$, $\widehat{\omega}[n]$, $\widehat{\alpha}[n]$ are denoted, respectively, by $H_\phi(z)$, $H_\omega(z)$, and $H_\alpha(z)$, and the corresponding impulse responses by $h_\phi[n]$, $h_\omega[n]$, and $h_\alpha[n]$. These can be easily found from $\mathbf{G}_\phi(z)$ and Fig. 3 and are omitted to save space.

For amplitude estimation, a similar strategy can be followed. The state matrix in this case is simply $\boldsymbol{A}_a = \mathbf{0}$. For zero-initial conditions, this observer is equivalent to a first-order filter

$$H_a(z) = \frac{k_4}{1 + (k_4 - 1)z^{-1}}$$

where k_4 is the gain parameter. However, to speed up convergence, the initial amplitude estimate is set to the nominal amplitude value. The corresponding impulse response is $h_a[n]$.

D. Predictor

It must be considered that feedback is not instantaneous, at least a unit delay must be introduced in this path for the loop to be computable [28]. To compensate for this, a linear predictor based on the state model is included, yielding a familiar Taylor series approximation [20]

$$\widehat{\phi}[n+1|n] = \widehat{\phi}[n] + \widehat{\omega}[n]\, T + \widehat{\alpha}[n]\, \frac{T^2}{2}.$$

Of course, the error introduced by this approximation depends on the phase dynamics but it is always $O(T^3)$. For practical signals and values of T, it will be negligible. Instead, if no predictor is used the error would be $O(T)$ which could be unacceptable in terms of TVE. For example, for $B = 2\pi \times 10$ rad/s and $T = 1$ ms, TVE will be roughly 3%.

E. Parameter Selection

It is interesting to highlight the fact that the resulting structure resembles that of a limiting Kalman filter [29]. The main difference lies in the parameter selection criterion. While the Kalman gains are selected to minimize the estimation mean-square error, the choice here is based on a set of time and frequency response requirements.

In order to use available results from continuous-time type 3 PLLs theory, we need to define an appropriate mapping between continuous-time and discrete-time gains. Let $F(s) = g_1 + g_2/s + g_3/s^2$ be the loop filter transfer function of a continuous-time type 3 PLL. Then, using standard

$$\mathbf{G}_\phi(z) = \frac{1}{2(1-k_1)(1-z^{-1})^3} \begin{bmatrix} 2k_1 + (-4k_1 + 2k_2T + k_3T^2)z^{-1} + (2k_1 - 2k_2T + k_3T^2)z^{-2} \\ 2(1-z^{-1})[k_2 - (k_2 - k_3T)z^{-1}] \\ 2k_3(1-z^{-1})^2 \end{bmatrix} \tag{5}$$

approximations [28], it can be shown that

$$k_1 = \frac{g_1 T}{1 + g_1 T}, \quad k_2 = \frac{g_2 T}{1 + g_1 T}, \; k_3 = \frac{g_3 T}{1 + g_1 T}.$$

Thus, any suitable criterion for the selection of continuous-time gains may be used to choose discrete-time gains. In this paper, we will use the convenient parameterization of the gains, in terms of stability margins and bandwidth, presented in [27]. Although guidelines from [27] and [28] are quite useful, these are based on a single PLL without a PF stage. Due to the complex interaction between the two stages, a trial-and-error refinement was performed[5] with the aid of the properties presented in Section VII. It is noted that the required bandwidths for an appropriate dynamic response are much greater than the PF stopband frequency, which confirms the need of that stage for filtering interference signals.

VI. Narrowband Compensation Algorithm

For completeness, the NCA introduced in [17] is now briefly reviewed. It is based on two hypotheses: the positive-sequence signal of the fundamental component may be represented as a narrowband signal and the global group delay is constant in the frequency range of interest. For practical reasons, the effects of the analog stage are also included and lumped into an analog transfer function $H_{\mathrm{AS}}(s)$ which is then compensated along with the digital stage. In this paper, however, we consider only the integer delay PFs, so that the total delay is $\tau = mT$ with $m = N/2$, and $\phi_{\mathrm{PF}}(\omega T) = -\omega\tau$. Thus, the NCA equations simply reduce to a time alignment and gain compensation

$$\begin{aligned} &\widetilde{\alpha}[n] = \widehat{\alpha}[n+m], \quad \widetilde{\omega}[n] = \widehat{\omega}[n+m] \\ &\widetilde{\phi}[n] = \widehat{\phi}[n+m], \quad \widetilde{a}[n] = \widehat{a}[n+m]/G_{\mathrm{PF}}(\widetilde{\omega}[n]T). \end{aligned} \tag{6}$$

These expressions are convenient for analysis purposes (they are used extensively in the Appendix). However, in a practical implementation, the original NCA equations should always be used to take into account the necessarily nonlinear phase of the analog stage frequency response.

VII. System Performance Properties

In this section, we will consider some properties of the system regarding its performance with respect to different situations contemplated in the IEEE Standard. They are important because they show which factors dominate performance metrics and are therefore useful for validation purposes and as design guidelines. It is assumed that the DSS-PLL parameters are selected appropriately, which basically means that bandwidth is sufficiently wide so that it does not distort in a significant way phase and amplitude information signals. This assumption, however, should be verified by numerical simulations. In any case, the results are useful to understand the error contribution of each stage of the system. Short proofs are provided in the Appendix.

The first property of the system is straightforward and refers to its convergence for the stationary case. Note that this result implies that the system performance, unlike many different methods, is independent of the input signal frequency.

Property 1: The system converges with no steady-state errors (TVE $\to$ 0, FE $\to$ 0, Rate of Change of Frequency Error (RFE) $\to$ 0) for a free interference sinusoidal balanced input signal.

Of course, when interference and/or unbalances are present, steady-state errors will not be equal to zero. It is shown that worst case TVE depends mainly on the PF stopband attenuation δ_s since gain peaking of $H_\phi(e^{j\nu})$ is generally small,[6] while for FE and RFE, the effect of the DSS-PLL becomes much more critical. Note, however, that these bounds are generally loose, that is, they are rarely attained. Nevertheless, they show which factors should be considered to reduce errors. The gain peaks decrease as either the parameter PM increases or ω_c decreases.

Property 2: The maximum TVE, FE, and RFE when an interference is present at the input may be bounded as

$$\begin{aligned} &\mathrm{TVE} \le \zeta\delta_s\sqrt{1 + \|H_\phi\|_\infty^2}, \quad \mathrm{FE} \le \frac{\zeta}{2\pi}\delta_s\|H_\omega\|_\infty, \\ &\mathrm{RFE} \le \frac{\zeta}{2\pi}\delta_s\|H_a\|_\infty \end{aligned} \tag{7}$$

where ζ is the ratio between the interference and signal amplitudes at the input, and $\|H(e^{j\nu})\|_\infty = \max_\nu |H(e^{j\nu})|$.

For modulated signals, as expected, the main factor that affects TVE is the PF passband ripple δ_p. For phase modulated signals, we also provide FE and RFE bounds which show that the errors arise mainly from the nonideal characteristics of $H_\omega(e^{j\nu})$ and $H_\alpha(e^{j\nu})$ in the modulation frequency band.

Property 3: The maximum TVE for amplitude modulated signals is dominated by the AE and it may be approximately bounded as follows:

$$\mathrm{TVE} \le \frac{2k_a}{1 - k_a}\delta_p \tag{8}$$

where k_a is the modulation factor. On the other hand, as in the stationary case, PE $\to$ 0, FE $\to$ 0, and RFE $\to$ 0. For phase modulated signals, the maximum TVE, FE, and RFE satisfy

$$\begin{aligned} &\mathrm{TVE} \le 2J_0(k_\phi)\delta_p, \qquad \mathrm{FE} \approx \frac{J_1(k_\phi)}{\pi J_0(k_\phi)}\left|H_\omega(e^{j\nu_m}) - j\frac{\nu_m}{T}\right|, \\ &\mathrm{RFE} \approx \frac{J_1(k_\phi)}{\pi J_0(k_\phi)}\left|H_\alpha(e^{j\nu_m}) + \frac{\nu_m^2}{T^2}\right| \end{aligned} \tag{9}$$

where J_k is the kth order Bessel function of the first kind [30], ν_m is the discrete-time modulation frequency, and k_ϕ is the phase modulation factor.

Frequency ramp signals are much harder to analyze in detail. However, it is clear that the TVE will be mainly due to the PF distortion since, as mentioned earlier, a type 3 PLL can track perfectly these types of signals. The main factor that affects this level of distortion is the PF passband edge

[5]The results are a phase margin of PM = 85° and a crossover frequency of $\omega_c = 2\pi$ 100 for the M class PMU, so that $k_1 = 0.3094$, $k_2 = 16.9737$, and $k_3 = 465.6382$, while PM = 70° and $\omega_c = 2\pi$ 100 for the P class PMU, so that $k_1 = 0.3033$, $k_2 = 67.1972$, $k_3 = 7.4447 \times 10^3$. The amplitude parameter k_4 may be chosen simply as $1 - e^{pT}$, where p is the corresponding continuous-time pole. In both cases, we set $p = -2\pi \times 500$ rad/s, so that we obtained $k_4 = 0.8940$.

[6]Of course, this assumption can be controlled and checked by the system designer. In any case, a high gain peaking value is undesirable.

frequency f_p, so it is clearly more critical to the M class PMU requirements. Frequency and ROCOF errors will also be dependent on the characteristics of the DSS-PLL.

With respect to step signals, we present approximations of phase and amplitude overshoots (AOs) as simple functions of $h_{\mathrm{PF}}[n]$ and some remarks about TVE, FE, and RFE response times.

Property 4: Phase overshoot (PO) and AO may be approximated by

$$\mathrm{PO} \approx \mathrm{AO} \approx \frac{\max\limits_{N/2 \le l \le N-1} \sum_{k=0}^{l} h_{\mathrm{PF}}[k]}{\sum_{k=0}^{N} h_{\mathrm{PF}}[k]} - 1. \tag{10}$$

Moreover, the TVE response time ($t_{r,\mathrm{TVE}}$) depends primarily on the spread of $h_{\mathrm{PF}}[n]$. For the amplitude step, FE and RFE response times ($t_{r,\mathrm{FE}}$ and $t_{r,\mathrm{RFE}}$) are theoretically zero. Instead, for the phase step test, $t_{r,\mathrm{FE}}$ and $t_{r,\mathrm{RFE}}$ depend on the spread of the functions $h_{\mathrm{PF},\omega}[n] = (h_{\mathrm{PF}} * h_{\omega})[n]$ and $h_{\mathrm{PF},\alpha}[n] = (h_{\mathrm{PF}} * h_{\alpha})[n]$, respectively.

VIII. Numerical Results

In this section, we present the performance of the proposed system under the most stringent tests required by the IEEE Standard with respect to the metrics defined therein. Furthermore, we will check the properties presented in Section VII. Both an M ($F_s = 10$ fps) and P ($F_s = 50$ fps) class PMUs case studies are considered. Nominal frequency is $f_0 = 50$ Hz and sampling period is $T = (28 \times 50)^{-1}$ s. The PF parameters are presented in Section IV and they were implemented in four stages for the M class PMU and two stages for the P class PMU. The DSS-PLL parameters are presented in Section V. The system effective delay is 530.7 ms for the M class PMU and 32.1 ms for the P class PMU and both are below the IEEE Standard latency limit.

A. Stationary Tests

1) Balanced Signals: First, both systems are tested with a sinusoidal input signal with frequency $f = 52$ Hz, which represents the boundary of the passband. After convergence, negligible errors (TVE $\sim 10^{-10}$%, FE $\sim 10^{-11}$ Hz, and RFE $\sim 10^{-9}$ Hz/s) are obtained. Similar results are obtained for $f = 48$ Hz and a frequency sweep simulation confirms that performance is independent of the input signal frequency as established by Property 1.

Second, harmonic interference rejection is evaluated at a total harmonic distortion level of 10% for the M class PMU and 1% for the P class PMU for the first 12 harmonics. In Fig. 4, TVE versus harmonic number is shown. Worst case TVE, FE, and RFE are given in Table II. The simple bounds found from Property 2 are[7]: TVE ≤ 0.1514%, FE ≤ 0.0095 Hz, and RFE ≤ 0.2510 Hz/s for the M class PMU, while TVE ≤ 0.0190%, FE ≤ 0.0045 Hz, and RFE ≤ 0.4841 Hz/s for the P class PMU. Clearly, these are rather loose bounds and can not properly explain the differences that arise in the results due to the interaction of the PF and the DSS-PLL. Note, however, that much more accurate bounds can be found with more complex calculations (see the Appendix). For the M class PMU, out of band interference is evaluated by adding a disturbance at frequency $f_i = f_0 + Fs/2 = 55$ Hz with a total interharmonic distortion of 10%. By varying the fundamental frequency in the passband, the TVE behaves as shown in Fig. 5. Worst case TVE, FE, and RFE for a joint sweep of the signal and the interference frequencies in their full ranges are presented in Table III. Note that in this case the bounds from Property 2 are much tighter.

Finally, we have tested both systems with additive white Gaussian noise at an SNR between 40 and 80 dB. Results of the mean and standard deviation of the TVE, FE, and RFE as a function of SNR are shown in Fig. 6. They show that both systems are robust against noise for realistic SNR values.

[7]For reference, for the M class PMU: $\|H_\phi\|_\infty = 1.0460$, $\|H_\omega\|_\infty = 59.6322$, and $\|H_\alpha\|_\infty = 1.5772 \times 10^3$. For the P class PMU: $\|H_\phi\|_\infty = 1.2085$, $\|H_\omega\|_\infty = 284.2106$, and $\|H_\alpha\|_\infty = 3.0419 \times 10^4$.

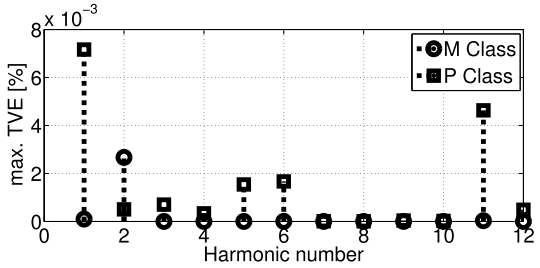

Fig. 4. TVE for the first 12 harmonics for both PMUs.

TABLE II
Harmonic Distortion Results

	M		P	
Metric	Result	Std. limit	Result	Std. limit
max. TVE [%]	0.0027	1	0.0072	1
max. FE [Hz]	1.79×10^{-4}	0.0050	0.0026	0.0050
max. RFE [Hz/s]	0.0050	-	0.2766	0.4000

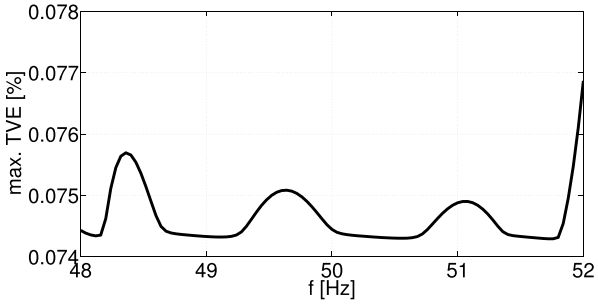

Fig. 5. TVE for the out-of-band interference test versus the fundamental frequency.

TABLE III
Out of Band Interference Test Results

Metric	Result	Std. limit
max. TVE [%]	0.0776	1.3
max. FE [Hz]	0.0066	0.01
max. RFE [Hz/s]	0.1675	-

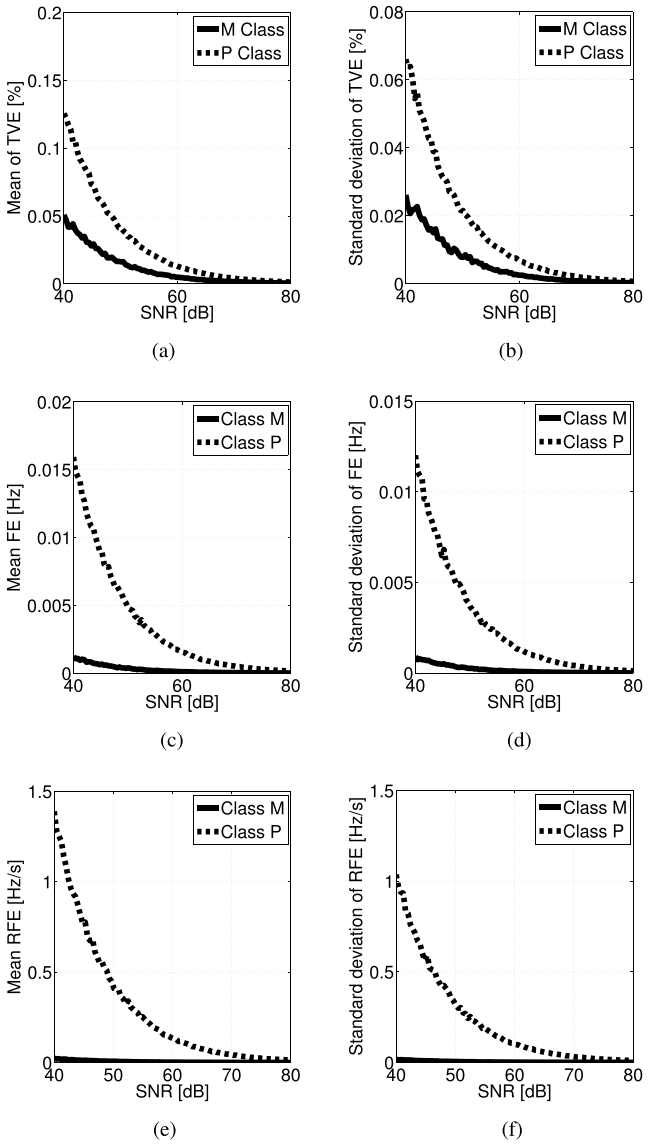

Fig. 6. TVE, FE, and RFE statistics as a function of SNR. (a) TVE mean. (b) TVE standard deviation. (c) FE mean. (d) FE standard deviation. (e) RFE mean. (f) RFE standard deviation.

It is also evident that the M class PMU is less sensitive to this disturbance. This is due to the fact that the noise bandwidths of both the PF and the DSS-PLL (a consequence of the higher PM value) estimators are smaller.

2) Unbalanced Signals: The system was tested with a fundamental negative-sequence and zero-sequence distortion at a 10% (M class) and 1% (P class) of the positive-sequence signal's amplitude and varying the fundamental frequency in the passband. Worst case results are shown in Table IV. As expected, both systems behave well (see Section III).

B. Dynamic Tests

1) Amplitude and Phase Modulation: The modulation frequency is set to 2 Hz, the amplitude modulation factor to 0.1 and the phase modulation factor to 0.1 rad. Results are as shown in Table V. The tracking capability is appreciated

TABLE IV
UNBALANCE DISTORTION RESULTS

	M		P	
Metric	Neg.-seq.	Zero-seq.	Neg.-seq.	Zero-seq.
max. TVE [%]	0.0047	$\sim 10^{-9}$	0.0022	$\sim 10^{-10}$
max. FE [Hz]	3.26×10^{-4}	$\sim 10^{-10}$	0.0006	$\sim 10^{-11}$
max. RFE [Hz/s]	0.0090	$\sim 10^{-9}$	0.0703	$\sim 10^{-9}$

TABLE V
MODULATION TEST RESULTS

	M			P		
Metric	Amp.	Phase	Std.	Amp.	Phase	Std.
max. TVE [%]	0.0111	0.1765	3	0.0148	0.0087	3
max. FE [Hz]	$\sim 10^{-11}$	0.0205	0.12	$\sim 10^{-13}$	0.0010	0.06
max. RFE [Hz/s]	$\sim 10^{-10}$	1.1647	2.30	$\sim 10^{-11}$	0.2739	2.30

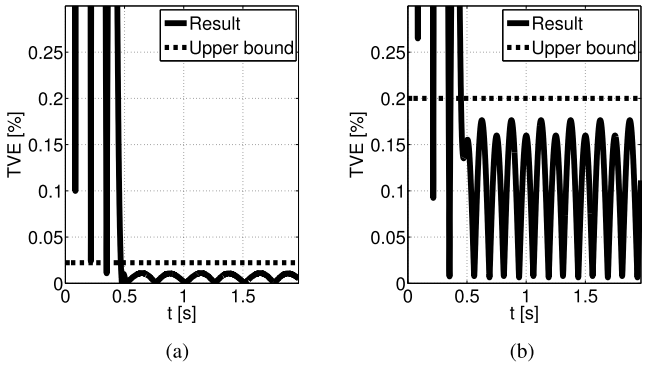

Fig. 7. TVE for modulation tests for the M class PMU. (a) TVE for amplitude modulation. (b) TVE for phase modulation.

TABLE VI
FREQUENCY RAMP RESULTS

	M		P	
Metric	Result	Std. limit	Result	Std. limit
max. TVE [%]	0.1090	1	0.0039	1
max. FE [Hz]	0.0005	0.01	0.0001	0.01
max. RFE [Hz/s]	0.0033	0.20	0.0129	0.42

in Fig. 7, where the TVE evolution is shown for both tests for the M class PMU. The TVE upper bound given by Property 3 for amplitude modulation is 0.0222%, while for phase modulation it is 0.1995%. Both bounds are found to be satisfactory. We also confirm that FE and RFE are negligible for the amplitude modulation tests. On the other hand, for the M class PMU, FE and RFE approximations for phase modulation are, respectively, 0.0205 Hz and 1.162 Hz/s, which are very accurate. Similar conclusions hold for the P class PMU.

2) Frequency Ramp: After 5 s of a pure sinusoidal signal, the ramp rate is set to 1 Hz/s, being the initial frequency 48 Hz and the final frequency 52 Hz. Performance obtained is shown in Table VI. As can be seen in Fig. 8 for the RFE evolution of each PMU, the DSS-PLL locks well within the exclusion interval. Note that the TVE for the M class PMU is much higher than that of the P class PMU, but the difference between

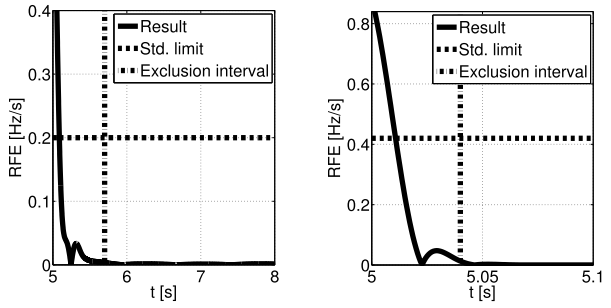

Fig. 8. RFE evolution for the frequency ramp test. (a) RFE for M class PMU. (b) RFE for P class PMU.

TABLE VII
STEP TEST RESULTS

	M			P		
Metric	Amp.	Phase	Std. limit	Amp.	Phase	Std. limit
Over. [%]	7.575	7.513	10	3.592	4.302	5
$t_{r,\mathrm{TVE}}$ [s]	0.119	0.330	0.70	0.018	0.020	0.04
$t_{r,\mathrm{FE}}$ [s]	0	0.822	1.40	0	0.089	0.09
$t_{r,\mathrm{RFE}}$ [s]	0	0.831	1.40	0	0.10	0.12

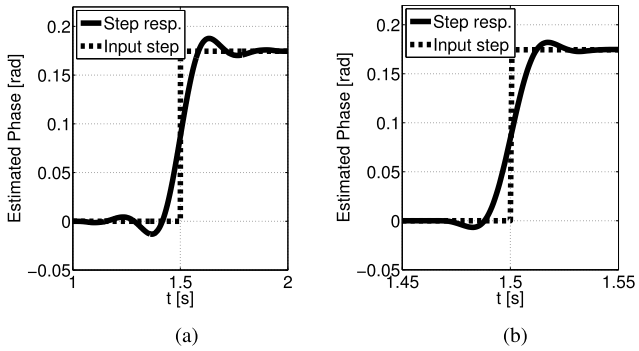

Fig. 9. Phase responses for the phase step test. (a) M class PMU. (b) P class PMU.

FE and RFE is much smaller, showing the effects of the different PF and DSS-PLL characteristics.

3) Step Tests: Amplitude step size is set to 10% of initial amplitude value and phase step size to $\pi/18$ rad. Results for each separate test are shown in Table VII, with their respective response times. To illustrate these results, the phase step response of both PMUs is shown in Fig. 9. Approximations of overshoot given in Property 4 are PO $\approx$ AO $=$ 7.5754% for the M class PMU and PO $\approx$ AO $=$ 3.6007% for the P class PMU. Note that for the P class PMU the PO approximation is less accurate which shows that the PLL has a nonnegligible impact on the step response. For the amplitude step, the approximations of $t_{r,\mathrm{TVE}}$ as functions of $h_{\mathrm{PF}}[n]$ are 0.118 s (M class) and 0.016 s (P class), while for the phase step, they are 0.328 s (M class) and 0.019 s (P class). These results confirm the usefulness of Property 4. Correct delay compensation is confirmed because the step time delay is less than the sampling period. Also, as expected, frequency and ROCOF are the most sensitive estimates to phase jumps in that their transients are longer, specially for the P class PMU. To reduce these response times, the bandwidth of the DSS-PLL needs to be increased thus degrading the harmonic rejection capability. To counteract this, a more complex PF may be used. The limit of this strategy is, of course, the system delay constraint of the IEEE Standard.

IX. CONCLUSION

A complete design of a PMU digital stage was presented along with its validation through numerical simulations for both an M and P class designs. The approach taken was modular, that is, we decouple the estimation problem into demodulation, filtering, dynamic tracking, and compensation. The advantage of this is that each block can be designed almost independently of each other.

This paper applies the Park transform as a three-phase demodulation scheme makes the system robust against signal unbalances. On the other hand, the importance of linear phase in the filtering stage of the system was emphasized, and we showed how small the group delay dispersion in the pass-band region should be for the proper operation of the PMU. A minimax linear-phase FIR PF design was presented as a benchmark and a detailed analysis of multistage designs was carried to show the existing tradeoff between computational cost, delay, and memory requirements which are necessary to consider carefully in an actual implementation of the system. An extension of the SRF-PLL based on the estimator-predictor approach was proposed. Basically, the loop filter design is based on a state-space model instead of the standard PI controller. This revealed how to estimate frequency and ROCOF inside the loop and pave the way for future improvements. It also contributes to the digitalization strategy, since the phase predictor was shown to be of paramount importance. Important properties of the system were derived analytically, which showed the existing tradeoffs between tracking and filtering that is an inherent problem of all the PLL-based structures and other PMU algorithms. It was verified that the desired relaxation of the requirements was achieved by the addition of the linear-phase PF, at the expense of some amount of delay and computational resources. Finally, we have applied the recently introduced narrowband compensation algorithm. It is worth to emphasize that all the requirements of the IEEE Standard were met.

Despite we did not perform a detailed analysis of the computational cost of the entire system, we would like to mention the dominant factors for each stage. The cost of the 3PD is mainly given by the evaluation of the matrix $\boldsymbol{P}[n]$, which involves computation of trigonometric functions. The cost of the PF depends strongly on the transition bandwidth Δf [see (3) and the discussion following it], although the multistage strategy makes this dependence much less severe. Note that this is the only computational difference between different PMU types (class and reporting rate). The cost of the DSS-PLL is primarily given by that of the RT and APD computations, which again requires the computation of trascendental functions. Finally, for the NCA block, the cost of evaluating the gain and phase responses clearly prevails over the rest of the computations.

To wrap up, we would like to comment on two possible extensions of this paper. First, as mentioned in Section IV, there is the possibility of using quasi-linear-phase IIR filters designed with the optimization methods. This approach may give important improvements in both the delay and computational requirements of the filter or, conversely, better filtering performance for the same requirements. Second, while the DSS-PLL has a strong theoretical motivation as a linear observer, it provides coupled estimations of phase, frequency, and ROCOF. This certainly limits its possibilities. A more flexible approach would be to design independently the three loop filters.

APPENDIX
PROOFS OF SYSTEM PROPERTIES

In this Appendix, we present brief proofs for the system properties established in Section VII. An assumption that is used repeteadly to simplify the analysis is that the bandwidths of $H_a(e^{j\nu})$, $H_\phi(e^{j\nu})$, $H_\omega(e^{j\nu})$, and $H_\alpha(e^{j\nu})$ are much larger than that of $H_{\rm PF}(e^{j\nu})$ due to the dynamic response requirements (large bandwidth hypothesis). However, it is noted that this assumption is not always accurate and should always be checked by computer calculations.

Property 1: In this case, the balanced input signal may be characterized by $a_1[n] = a_1$ and $\phi_1[n] = \nu_s n + \phi_1$ where $\nu_s = \Delta\omega_s T$. Therefore, a straightforward calculation shows that $a[n] = G_{\rm PF}(\nu_s)a_1$ and $\phi[n] = \nu_s(n-m) + \phi_1$. Starting from the phase loop, and analyzing the difference equations relating $\phi[n]$ with $\widehat{\phi}[n]$, $\widehat{\omega}[n]$, and $\widehat{\alpha}[n]$, we find after simple but tedious calculations that $\widehat{\phi}[n] = \phi[n]$, $\widehat{\omega}[n] = \nu_s/T = \Delta\omega_s$, and $\widehat{\alpha}[n] = 0$. Therefore, $\widetilde{\alpha}[n] = 0$, $\widetilde{\omega}[n] = \Delta\omega_s$, and $\widetilde{\phi}[n] = \widehat{\phi}[n+m] = \nu_s n + \phi_1 = \phi_1[n]$. On the other hand, since $u_a[n] = a[n]$ is a constant and $H_a(z=1) = 1$, we have $\widehat{a}[n] = G_{\rm PF}(\nu_s)a_1$. Finally, since frequency is estimated with no error $G_{\rm PF}(\widetilde{\omega}[n]T) = G_{\rm PF}(\nu_s)$ so that $\widetilde{a}[n] = a_1 = a_1[n]$.

Property 2: We consider a positive-sequence interference signal without loss of generality. In this case, the input signal is the sum of two positive-sequence signals. The first one is the fundamental component and is characterized by $a_1[n]$ and $\phi_1[n]$ as in Property 1. The second one is the interference component and is characterized by $b_1[n] = b_1$ and $\theta_1[n] = \nu_i n + \theta_1$ where $\nu_i = \Delta\omega_i T$. Proceeding as in Property 1 with each term, it can be shown that the outputs of the APD block are: $u_a[n] \approx a_1' + b_1'\cos(\psi[n])$, and $u_\phi[n] \approx \phi_1'[n] + r\sin(\psi[n]) - \widehat{\phi}_p[n]$. Here, we have defined $a_1' = G_{\rm PF}(\nu_s)a_1$, $\phi_1'[n] = \nu_s(n-m) + \phi_1$, $b_1' = G_{\rm PF}(\nu_i)b_1$, $\theta_1'[n] = \nu_i(n-m) + \theta_1$, $r = b_1'/a_1'$, and $\psi[n] = \theta_1'[n] - \phi_1'[n]$. Note that these are the first-order approximations in r, which are justified since the PFs ensure that $r \ll 1$.

We start by analyzing the amplitude estimation. By the large bandwidth hypothesis, we consider[8] $G_a(\nu_i - \nu_s) \approx 1$. We also assume that the PF has a sufficiently smooth magnitude response in the passband and the estimation $\widetilde{\omega}[n]$ is good enough, so that $|G_{\rm PF}(\widetilde{\omega}[n]T) - G_{\rm PF}(\nu_s)| \ll \delta_p$. Therefore, a worst case condition is $G_{\rm PF}(\widetilde{\omega}[n]T) \approx G_{\rm PF}(\nu_s) = 1 - \delta_p$. On the other hand, $G_{\rm PF}(\nu_i) \le \delta_s$. Moreover, note that $\delta_s/(1-\delta_p) \approx \delta_s$. Thus, $\widetilde{a}[n] \le a_1(1+\delta_s\zeta)$, where $\zeta = b_1/a_1$.

Now, we turn to the analysis of the phase estimation. Note that since $\psi[n]$ does not depend on $\widehat{\phi}_p[n]$, the term $r\sin(\psi[n])$ is a disturbance affecting directly the signal phase $\phi_1'[n]$. Then, using Property 1 and proceeding as earlier, we obtain: $\widetilde{\phi}[n] \le \phi_1[n] + \delta_s\zeta\|H_\phi\|_\infty$, where $\|H\|_\infty = \max_\nu |H(e^{j\nu})|$ is the usual infinity norm. After simple approximations, we finally obtain the bound for TVE, as given by (7). We can proceed similarly for frequency and ROCOF to obtain: FE $\le \zeta/2\pi \ \max_{\nu_s,\nu_i} \ G_{\rm PF}(\nu_i)G_\omega(\nu_i - \nu_s)$, and RFE $\le \zeta/2\pi \ \max_{\nu_s,\nu_i} \ G_{\rm PF}(\nu_i)G_\alpha(\nu_i - \nu_s)$. Note that the maximum should be evaluated with respect to ν_s and ν_i in their respective ranges which are dependent on the PMU class and reporting rate. These are very accurate bounds, but provide little insight. More simple bounds are simply obtained as $\zeta\delta_s\|H_\omega\|_\infty/(2\pi)$ and $\zeta\delta_s\|H_\alpha\|_\infty/(2\pi)$, as given by (7). These are much simpler but looser bounds.

Property 3: For amplitude modulated signals, $a_1[n] = a_1[1 + k_a\cos(\nu_m n + \phi_m)]$, where $\nu_m = \omega_m T$ and $\phi_1[n] = \phi_1$. Therefore, a straightforward calculation shows that $a[n] = a_1[G_{\rm PF}(0) + k_a G_{\rm PF}(\nu_m)\cos(\nu_m(n-m) + \phi_m)]$ and $\phi[n] = \phi_1$. The phase loop analysis is a particular case of the one made for Property 1 (set $\Delta\omega_s = 0$) so that phase, frequency, and ROCOF converge without error. Besides, we have $\widehat{a}[n] \approx a[n]$ due to the large bandwidth hypothesis. Then, since $\widetilde{a}[n] \approx a[n+m]/G_{\rm PF}(0)$, we obtain

$$\mathrm{TVE}[n] = \left|\frac{G_{\rm PF}(\nu_m)}{G_{\rm PF}(0)} - 1\right| \frac{|k_a\cos(\nu_m n + \phi_m)|}{|1 + k_a\cos(\nu_m n + \phi_m)|}.$$

Finally, note that the first factor is approximately bounded by $2\delta_p$, while the second is bounded by $k_a/(1-k_a)$. This yields the desired bound given by (8).

On the other hand, for a phase modulated signal, we have $a_1[n] = a_1$ and $\phi_1[n] = k_\phi\cos(\theta_m)$, with $\theta_m = \nu_m n + \phi_m$. Thus, for small values of k_ϕ, we have [30]

$$\mathbf{x}_{dq}[n] \approx a_1 \begin{bmatrix} J_0(k_\phi) - 2J_2(k_\phi)\cos(2\theta_m) \\ 2J_1(k_\phi)\cos(\theta_m) - 2J_3(k_\phi)\cos(3\theta_m) \end{bmatrix}$$

where J_k is the kth order Bessel function of the first kind.

The expressions for $y_d[n]$ and $y_q[n]$ are simply obtained but are omitted here for space reasons. By expanding on the variable $y_q[n]/y_d[n]$, we readily find the following approximations: $a[n] \approx y_d[n]$ and $\phi[n] \approx y_q[n]/y_d[n] \approx y_q[n]/J_0(k_\phi)$. Expressions for the estimates are readily found by using the usual worst case considerations. Using the large bandwidth hypothesis, we obtain the following upper bounds for AE and PE upon retaining the dominant terms: AE $\le a_1 2J_0(k_\phi)\delta_p$ and PE $\le 4J_1(k_\phi)\delta_p/J_0(k_\phi)$. It is interesting to note that the AE bound is generally greater than the PE one. Finally, by noting that FE and RFE errors are primarily due to the DSS-PLL and thus neglecting the PFs stage, we obtain the approximations given in (9).

Property 4: For an amplitude step signal, $a_1[n] = a_1(1 + \Delta a\, u[n])$ and $\phi_1[n] = \phi_1$, where $u[n]$ is the unit step signal. Then, the outputs of the PFs have an amplitude $a[n] = a_1(G_{\rm PF}(0) + \Delta a\, s_{\rm PF}[n])$ and a phase $\phi[n] = \phi_1$, where $s_{\rm PF}[n] = (h_{\rm PF} * u)[n]$ is the step response of the PFs.

[8]This is a good approximation for interharmonic signals whose frequency is close to the fundamental. Otherwise, it is an upper bound.

Then, estimated amplitude is $\widehat{a}[n] = a_1(G_{\mathrm{PF}}(0)+\Delta a\, s_{\mathrm{PF},a}[n])$, where $s_{\mathrm{PF},a}[n] = (h_a * s_{\mathrm{PF}})[n]$. By the large bandwidth hypothesis, we have $s_{\mathrm{PF},a}[n] \approx s_{\mathrm{PF}}[n]$. As we now from Property 1, phase, frequency, and ROCOF are estimated with no error. Therefore, $\widetilde{a}[n] \approx a_1\{1 + \Delta a\, s_{\mathrm{PF}}[n+m]/G_{\mathrm{PF}}(0)\}$. The AO is given by $\mathrm{AO} = \max_{n\geq 0}\{\widetilde{a}[n] - a_1(1+\Delta a)\}/a_1(1+\Delta a)$. Since $G_{\mathrm{PF}}(0) = \sum_{k=0}^{N} h_{\mathrm{PF}}[k]$ and $s_{\mathrm{PF}}[n+m] = \sum_{k=0}^{n+m} h_{\mathrm{PF}}[k]$, we readily obtain (10). The TVE, FE, and RFE response times properties follow immediately.

For a phase step signal, we have $a_1[n] = a_1$ and $\phi_1[n] = \Delta\phi\, u[n]$. The output of the PFs can be conveniently found by considering the response to the signal $a_1 e^{j\,\Delta\phi u[n]}$ and then taking real and imaginary parts for the d and q components. Therefore, for small $\Delta\phi$, we find $\phi[n] \approx \Delta\phi\, s_{\mathrm{PF}}[n]/G_{\mathrm{PF}}(0)$. The estimated and compensated phase is then $\widetilde{\phi}[n] \approx \Delta\phi\, s_{\mathrm{PF},\phi}[n+m]/G_{\mathrm{PF}}(0)$, where $s_{\mathrm{PF},\phi}[n] = (h_\phi * s_{\mathrm{PF}})[n]$. The PO is given by $\mathrm{PO} = \max_{n\geq 0}(\widetilde{\phi}[n] - \Delta\phi)/\Delta\phi$. By the large bandwidth hypothesis $s_{\mathrm{PF},\phi}[n] \approx s_{\mathrm{PF}}[n]$, and we obtain again (10). On the other hand, $\widetilde{\omega}[n] \approx \Delta\phi\, s_{\mathrm{PF},\omega}[n+m]/G_{\mathrm{PF}}(0)$ and $\widetilde{\alpha}[n] \approx \Delta\phi\, s_{\mathrm{PF},\alpha}[n+m]/G_{\mathrm{PF}}(0)$, where we have defined $s_{\mathrm{PF},\omega}[n] = (h_\omega * s_{\mathrm{PF}})[n]$ and $s_{\mathrm{PF},\alpha}[n] = (h_\alpha * s_{\mathrm{PF}})[n]$. The TVE, FE, and RFE response times properties are again direct.

REFERENCES

[1] G. Giannakis, V. Kekatos, N. Gatsis, S.-J. Kim, H. Zhu, and B. Wollenberg, "Monitoring and optimization for power grids: A signal processing perspective," *IEEE Signal Process. Mag.*, vol. 30, no. 5, pp. 107–128, Sep. 2013.

[2] *IEEE Standard for Synchrophasor Measurements for Power Systems*, IEEE Standard C37.118.1-2011 (Revision of IEEE Standard C37.118-2005), Dec. 2011.

[3] *IEEE Standard for Synchrophasor Measurements for Power Systems—Amendment 1: Modification of Selected Performance Requirements*, IEEE Standard C37.118.1a-2014 (Amendment to IEEE Standard C37.118.1-2011), Apr. 2014.

[4] A. Phadke and J. Thorp, *Synchronized Phasor Measurements and Their Applications* (Power Electronics and Power Systems). New York, NY, USA: Springer, 2008.

[5] D. Macii, D. Petri, and A. Zorat, "Accuracy analysis and enhancement of DFT-based synchrophasor estimators in off-nominal conditions," *IEEE Trans. Instrum. Meas.*, vol. 61, no. 10, pp. 2653–2664, Oct. 2012.

[6] D. Belega and D. Petri, "Accuracy analysis of the multicycle synchrophasor estimator provided by the interpolated DFT algorithm," *IEEE Trans. Instrum. Meas.*, vol. 62, no. 5, pp. 942–953, May 2013.

[7] J. A. de la O Serna, "Dynamic phasor estimates for power system oscillations," *IEEE Trans. Instrum. Meas.*, vol. 56, no. 5, pp. 1648–1657, Oct. 2007.

[8] W. Premerlani, B. Kasztenny, and M. Adamiak, "Development and implementation of a synchrophasor estimator capable of measurements under dynamic conditions," *IEEE Trans. Power Del.*, vol. 23, no. 1, pp. 109–123, Jan. 2008.

[9] J. A. de la O Serna and K. Martin, "Improving phasor measurements under power system oscillations," *IEEE Trans. Power Syst.*, vol. 18, no. 1, pp. 160–166, Feb. 2003.

[10] M. Platas-Garza and J. de la O Serna, "Dynamic phasor and frequency estimates through maximally flat differentiators," *IEEE Trans. Instrum. Meas.*, vol. 59, no. 7, pp. 1803–1811, Jul. 2010.

[11] P. Castello, M. Lixia, C. Muscas, and P. Pegoraro, "Impact of the model on the accuracy of synchrophasor measurement," *IEEE Trans. Instrum. Meas.*, vol. 61, no. 8, pp. 2179–2188, Aug. 2012.

[12] G. Barchi, D. Macii, and D. Petri, "Synchrophasor estimators accuracy: A comparative analysis," *IEEE Trans. Instrum. Meas.*, vol. 62, no. 5, pp. 963–973, May 2013.

[13] G. Barchi, D. Macii, D. Belega, and D. Petri, "Performance of synchrophasor estimators in transient conditions: A comparative analysis," *IEEE Trans. Instrum. Meas.*, vol. 62, no. 9, pp. 2410–2418, Sep. 2013.

[14] M. Karimi-Ghartemani, B.-T. Ooi, and A. Bakhshai, "Application of enhanced phase-locked loop system to the computation of synchrophasors," *IEEE Trans. Power Del.*, vol. 26, no. 1, pp. 22–32, Jan. 2011.

[15] M. Karimi-Ghartemani, *Enhanced Phase-Locked Loop Structures for Power and Energy Applications* (IEEE Press Series on Microelectronic Systems). Hoboken, NJ, USA: Wiley, 2014.

[16] P. Rodriguez, J. Pou, J. Bergas, J. Candela, R. Burgos, and D. Boroyevich, "Decoupled double synchronous reference frame PLL for power converters control," *IEEE Trans. Power Electron.*, vol. 22, no. 2, pp. 584–592, Mar. 2007.

[17] F. Messina, L. Rey Vega, C. G. Galarza, and H. Laiz, "An accurate phase compensation algorithm for PMUs," in *Proc. Conf. Precision Electromagn. Meas. (CPEM)*, Ottawa, ON, Canada, Jul. 2016.

[18] M. Karimi-Ghartemani and H. Karimi, "Processing of symmetrical components in time-domain," *IEEE Trans. Power Syst.*, vol. 22, no. 2, pp. 572–579, May 2007.

[19] M. Karimi-Ghartemani, S. Khajehoddin, P. Jain, and A. Bakhshai, "Derivation and design of in-loop filters in phase-locked loop systems," *IEEE Trans. Instrum. Meas.*, vol. 61, no. 4, pp. 930–940, Apr. 2012.

[20] J. I. Statman and W. J. Hurd, "An estimator-predictor approach to PLL loop filter design," *IEEE Trans. Commun.*, vol. 38, no. 10, pp. 1667–1669, Oct. 1990.

[21] J. A. de la O Serna, "Synchrophasor measurement with polynomial phase-locked-loop Taylor–Fourier filters," *IEEE Trans. Instrum. Meas.*, vol. 64, no. 2, pp. 328–337, Feb. 2015.

[22] S. Toscani and C. Muscas, "A space vector based approach for synchrophasor measurement," in *Proc. IEEE Int. Instrum. Meas. Technol. Conf. (I2MTC)*, May 2014, pp. 257–261.

[23] R. C. Nongpiur, D. J. Shpak and A. Antoniou, "Improved design method for nearly linear-phase IIR filters using constrained optimization," *IEEE Trans. Signal Process.*, vol. 61, no. 4, pp. 895–906, Feb. 2013.

[24] A. Oppenheim and R. Schafer, *Discrete-Time Signal Processing* (Prentice-Hall Signal Processing Series). Upper Saddle River, NJ, USA: Pearson Education, 2011.

[25] P. Vaidyanathan, *Multirate Systems and Filter Banks* (Electrical Engineering. Electronic and Digital Design). London, U.K.: Dorling Kindersley, 1993.

[26] J. Lee and C. Un, "Performance analysis of digital tanlock loop," *IEEE Trans. Commun.*, vol. 30, no. 10, pp. 2398–2411, Oct. 1982.

[27] S. Golestan, M. Monfared, F. Freijedo, and J. Guerrero, "Advantages and challenges of a type-3 PLL," *IEEE Trans. Power Electron.*, vol. 28, no. 11, pp. 4985–4997, Nov. 2013.

[28] F. Gardner, *Phaselock Techniques*. Hoboken, NJ, USA: Wiley, 2005.

[29] C. Chui and G. Chen, *Kalman Filtering With Real-Time Applications* (Springer Series in Information Sciences). Berlin, Germany: Springer, 2013.

[30] M. Abramowitz and I. Stegun, *Handbook of Mathematical Functions: With Formulas, Graphs, and Mathematical Tables* (Applied Mathematics Series). New York, NY, USA: Dover, 1964. [Online]. Available: https://books.google.com.ar/books?id=MtU8uP7XMvoC

Francisco Messina (S'16) received the B.Sc. and M.Sc. degrees in electrical engineering from the University of Buenos Aires, Buenos Aires, Argentina, in 2014, where he is currently pursuing the Ph.D. degree with the Department of Electronics, School of Engineering.

He is currently with the Department of Electronics, School of Engineering, University of Buenos Aires, as a Teaching Assistant. His current research interests include phasor measurement unit algorithms and signal processing for power system applications.

Pablo Marchi (S'16) received the B.Sc. and M.Sc. degrees in electrical engineering from the University of Buenos Aires, Buenos Aires, Argentina, in 2014, where he is currently pursuing the Ph.D. degree with the Department of Electronics, School of Engineering.

His current research interests include phasor measurement unit algorithms and signal processing for power system applications.

Leonardo Rey Vega (S'07–M'11) received the M.Sc. (Hons.) and the Ph.D. (*summa cum laude*) degrees in electrical engineering from the University of Buenos Aires, Buenos Aires, Argentina, in 2004 and 2010, respectively.

From 2007 to 2008, he was invited from the INRS-Énergie, Matériaux et Télécommunications, Montréal, QC, Canada, and in 2012 he was a Visitor with the Department of Telecommunications, Supélec, France. He is currently an Assistant Professor with the University of Buenos Aires. His current research interests include statistical signal processing for smart-grid applications, information theory, and wireless sensor networks.

Cecilia G. Galarza received the Ingeniera degree in electrónica from the University of Buenos Aires, Buenos Aires, Argentina, in 1990, and the M.S. degree in electrical engineering and Ph.D. degree in computer science from the University of Michigan, Ann Arbor, MI, USA, in 1995 and 1998, respectively.

She was with Voyan Technologies, Santa Clara, CA, USA. She is also a Researcher with the National Council for Scientific and Technological Research (CONICET), Buenos Aires, Argentina, where she is with the Centro de Simulación Computacional. She is currently an Associate Professor with the School of Engineering, University of Buenos Aires. Her current research interests include systems engineering, systems for smart grid, and wireless networks.

Héctor Laiz was born in Argentina in 1964. He received the Diploma degree in electrical engineering from the University of Buenos Aires, Buenos Aires, Argentina, in 1988, and the Ph.D. degree from Technische Universität Braunschweig, Braunschweig, Germany, in 1999.

In 1989, he was with the Instituto Nacional de Tecnologia Industrial (INTI), National Metrology System of Argentina, where he was involved in the development of power and ac–dc transfer standards. He has been a Guest Scientist with Physikalisch-Technische Bundesanstalt, Braunschweig, Germany, and with the National Institute of Standards and Technology, Gaithersburg, MD, USA, where he was involved in highly accurate low frequency ac measurements. From 1999 to 2010, he was a Deputy Director of Metrology with INTI, dealing with scientific and legal metrology, where he is the Director of Metrology, Quality, and Environment, since 2010. In 2014 he was elected as President of the Inter-American Metrology System.